Silica Self-Assembly and the Synthesis of Microporous and Mesoporous Silicates

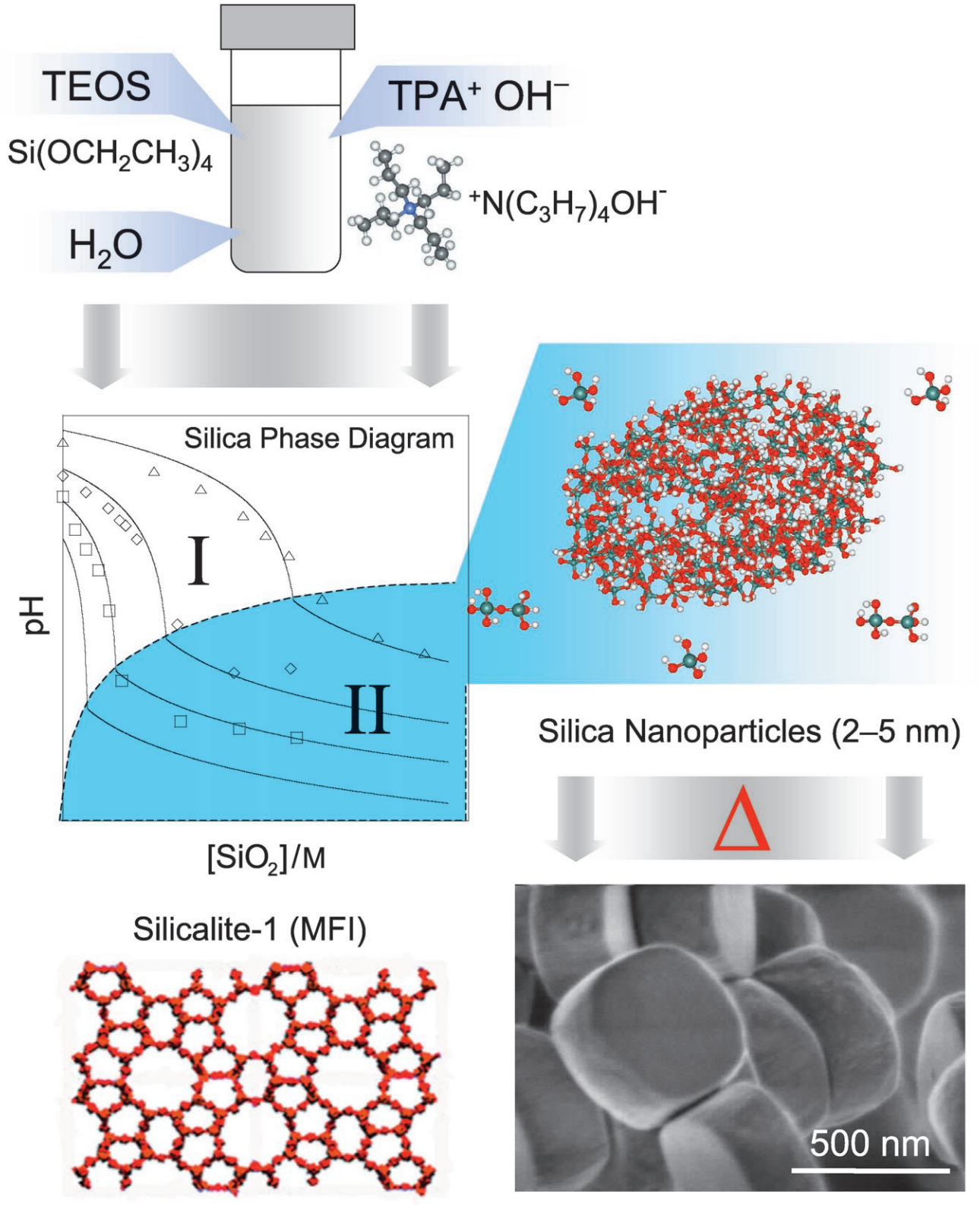

DOI: 10.1002/chem.200500684

Silica Self-Assembly and Synthesis of Microporous and Mesoporous Silicates

Jeffrey D. Rimer, Joseph M. Fedeyko, Dionisios G. Vlachos,* and Raul F. Lobo*[a]

Abstract: The microstructure of silica in basic aqueous solutions containing organic cations and prepared from monomeric precursors is reviewed and interpreted within the context of classical ideas of self-assembly of molecular aggregates. The solution properties can be understood by using the pseudo-phase separation approach coupled to the acid–base chemistry of silanol groups and the Poisson–Boltzmann equation. The silica nanoparticles frequently observed in these systems have a core–shell structure with silica in the core and the organic cations at the shell. Individual particles are observed when the forces between particles are repulsive—as is the case for small cations such as tetramethylammonium or tetrapropylammonium—and extended structures such as M41S materials are formed when the forces are attractive—-as is the case for surfactants such as cetyltrimethylammonium. These ideas are useful to understand the evolution of zeolite synthesis gels from nucleation to crystal growth. Although at room temperature the silica and the organic cations are segregated, upon heating the organic cations are embedded within the particles. This transformation signals the onset of structure direction whereby the size and geometry of the organic cation induce changes in the structure of silica that may lead to zeolite nuclei.

Keywords: aggregation · self-assembly · silicon · zeolites

Introduction

The synthesis of high-silica zeolites is a prototypic example of materials self-assembly with substantial commercial application.[1,2] In a representative protocol, a mixture containing a source of silica, water, a structure director (usually an organic cation) and a "catalyst" (usually a base) are heated to hydrothermal conditions (70–200 °C) under autogenous pressure to form, after hours or days, highly crystalline materials with exquisite structures. Upon removal of the organic structure director occluded in the pores (by heating in air), a microporous silica framework with remarkable chemical and physical properties is obtained.[3] The uniform pore size, thermal stability, and high acid site strength and density make zeolites one of the most versatile catalysts known to mankind.[4,5] Different zeolites can be prepared by changing the geometry and size of the structure director and by adding other inorganic components to the synthesis (such as Ge, Al, B, Be, Zn, etc.).[6] Although the success in preparing new frameworks by the zeolite community at large has been extraordinary—more than 26 new framework structures have been prepared in the last five years[7]—the molecular details by which these materials self-assemble (both during nucleation and crystal growth) have remained elusive.

During the last decade several groups have devoted intense efforts to determine the important molecular events that mark the evolution from a clear solution or an "amorphous" gel to a crystalline solid, and recently a more understandable picture of what is happening during the different stages of zeolite synthesis has started to emerge.[8–12] The focus has been the synthesis of silicalite-1 (Figure 1), using tetrapropylammonium hydroxide as the structure director, because it is easy to prepare, it is compositionally simple, and ZSM-5, its aluminosilicate analogue, is widely used in commercial catalytic processes.[5] The new insights—not only of value to those working on zeolites—have revealed fundamentally new aspects of silica chemistry and silica polymerization that should help those interested in the synthesis of mesoporous materials,[13] functional inorganic oxides and perhaps silica biomineralization.[14] In this Concept article we attempt to organize the results of these investigations to

[a] J. D. Rimer, J. M. Fedeyko, Prof. D. G. Vlachos, Prof. R. F. Lobo
Center for Catalytic Science and Technology
Department of Chemical Engineering
University of Delaware, Newark, DE 19716 (USA)
Fax: (+1) 302-831-1048
E-mail: vlachos@che.udel.edu
lobo@che.udel.edu

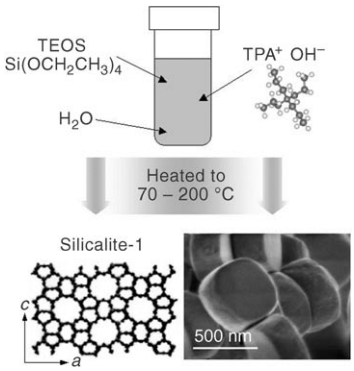

Figure 1. Schematic of the synthesis and structure of silicalite-1. A typical synthesis mixture will contain water, tetraethylorthosilicate (TEOS)- or other silica source such as Cabosil or Ludox colloidal silica- and tetrapropylammonium hydroxide (TPAOH). The synthesis gels usually contain SiO_2/TPAOH ratios of 3–4:1 and the composition of the final product is SiO_2/TPAOH 96:4 per unit cell. The structure of silicalite-1 contains straight and sinusoidal pores along the *a* and *b* directions and the organic cations sit at the intersections of this pore system. The pore windows are ~5.6 Å in diameter. Also shown is a scanning electron micrograph of a typical crystal morphology observed with TPA-silicalite-1 materials.

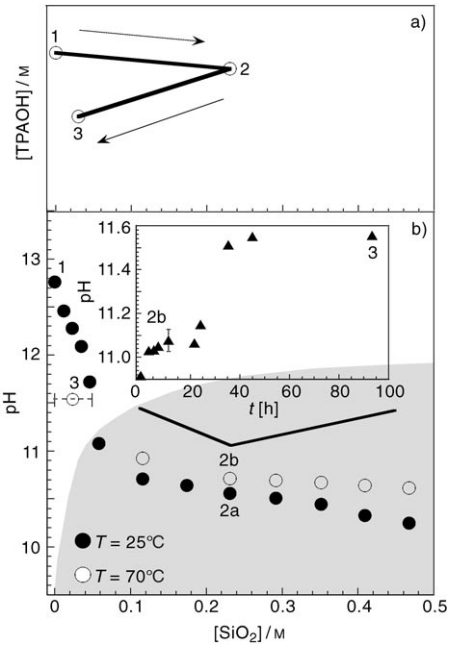

Figure 2. Operating line of a zeolite synthesis and its relation to pH for a solution with initial composition of TPAOH/H_2O 9:9500 (~0.05 M) as a function of the total concentration of SiO_2. The Figure illustrates changes in TPAOH composition (a) and pH (b) in the liquid phase as the reagents are mixed and heated under hydrothermal conditions. The 1→2a operating line is the mixing of the reagents and the 2b→3 operating line shows the actual crystallization of the zeolite. After nucleation, silica is progressively removed from the liquid phase until equilibrium is reached (point 3). The solid symbols are for solutions at room temperature, and the empty symbols are for solutions heated to 80 °C for a few hours. The inset in part (b) shows the *time* evolution of pH after the addition of 60 silicalite-1 nm seeds[15] to a solution of composition TPAOH/SiO_2/H_2O/C_2H_5OH 9:40:9500:160. The brackets on point 3 are used because the composition of the solution after crystallization is not known exactly. This is a compositionally simple zeolite synthesis since in most cases there is a source of aluminum (such as aluminum nitrate) and alkali-metal halides (usually NaCl).

provide a coherent summary of the molecular-level detail that is starting to appear from the work of various groups.

From Gel to Nuclei to Crystals

To help put things in context, we will summarize what is known to happen as we follow the operating line in a specific zeolite synthesis (Figure 2). We start at point 1 with a basic solution of tetrapropylammonium hydroxide, TPAOH (e.g., TPAOH/H_2O 9:9500 or ~0.05 M as in Figure 2). We add silica (in this case, tetraethylorthosilicate, TEOS) and move "instantaneously" to point 2a. Once the mixture is homogeneous, it is heated (point 2b) and after nucleation we move continuously from point 2b to point 3. Since there is an excess of structure director, the concentration of the organic cation decreases only slightly during crystallization. As one follows the properties of the solution along the operating line 1→2a, we note that the high pH initially drops because of the dissociation of silicic acid in solution but then it levels off and changes little with the addition of more TEOS (Figure 2b). Upon heating the solution (2a→2b), the pH increases slightly and after nucleation the solution composition approximately traces back the same operating conditions. As silica is consumed from the solution, the pH remains stable up to a specific point at which it rapidly starts to increase (inset of Figure 2b) until equilibrium is reached at low total concentration of silica in solution and high pH (point 3). The points in the curves of Figure 2b, where the slope of the pH changes (from 1→2 and from 2→3), are nearly the same. At point 3, equilibrium is reached and zeolite growth stops.

Along the 1→2a operating line, at the point that a drastic change in the slope of the pH is observed, other changes are also detected in the solution (Figure 3). The enthalpy of reaction of TEOS in TPAOH changes from −70 to −52 kJ mol^{-1} SiO_2,[16] and a change in the slope of the conductivity of the solutions is clearly observed. These changes in macroscopic properties are accompanied by a change in the microstructure of the solutions, as revealed by small angle X-ray and neutron scattering (SAXS and SANS). Figure 3c shows that before the change in slope, the SAXS pattern is essentially flat revealing the absence of any large silica species. After a SiO_2/TPAOH ratio of 1:1, the presence of silica nanoparticles is evident in the patterns and importantly, the nanoparticles change very little in size as more silica is added to the solution.[17] Further addition of TEOS increases the number density of particles but the particle size remains nearly constant.

The formation of silica nanoparticles, prior to and during the crystallization of silicalite-1, was reported by Schoeman over 10 years ago.[11,19] (silica nanoparticles in basic solutions are nothing new,[20] but the compositional range of stability is larger for small organic cations than for inorganic cations.)

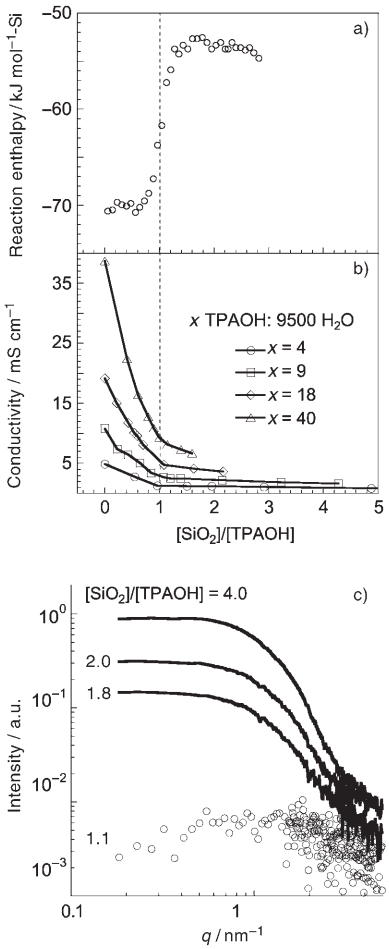

Figure 3. a) Reaction enthalpy of TEOS in TPAOH aqueous solutions with initial molar composition TPAOH/H_2O 9:480. The data are from ref. [16] with the abscissa normalized relative to the concentration of TPAOH to compare the solutions at different initial compositions. b) Conductivity of aqueous solutions of TPAOH (TPAOH/H_2O x:9500) as a function of the total concentration of silica.[17] c) SAXS patterns of silica/TPAOH solutions at different points in the curves of b) with $x = 9$.[18]

Since then, the role of these particles in the nucleation and growth of zeolites has been investigated extensively without conclusively determining how and whether particles are directly involved in the zeolite synthesis.[21–24] For our purposes, the key point is that the change in macroscopic properties of the solutions corresponds to the appearance of the nanoparticles as determined by SAXS and other techniques. The sudden appearance of nanoparticles at well-defined concentrations is very much analogous to the formation of micelles in aqueous solutions and the point of formation is thus called the critical aggregation concentration (cac).[25] A locus of cac for several organic and inorganic cations at different initial compositions has been determined experimentally and found to be independent of the identity of the cation.[18] This last observation indicates that silica nanoparticle formation is a rather general phenomenon independent of the actual process of zeolite crystallization.

Returning to Figure 2 (from point 2 to 3), a few hours after heating these TEOS/TPAOH solutions to ~90 °C, clear evidence of growing crystals is observed by SAXS,[9,26,27] calorimetry[28] and other techniques.[29] Upon nucleation, silica in solution starts to be depleted by the growing crystals and we start to move from point 2 to point 3. Figure 4 shows the heat evolution and pH during such a process,[30] where, interestingly, an exothermic region of crystal growth is rapidly followed by an endothermic region prior to the end of the synthesis. The pH remains nearly constant during the exothermic portion of crystal growth, but increases rapidly at the point at which the exothermic–endothermic transition is observed (see also inset in Figure 2b). Various reports show that during crystal growth silica nanoparticles remain in solution and their concentration decreases as crystallization progresses.[31] Material balances based on the data reported by Yang and Navrotsky[30] indicate that the point of transition from an exothermic to an endothermic process nearly coincides with the approximate location of the cac for the specific compositions investigated (Figure 4). It thus appears that the exothermic-endothermic transition is connected to the nature of silica in solution, that is, monomeric versus nanoparticles, which is used to grow the zeolite crystals. These measurements also indicate that it is possible to grow silicalite-1 crystals in the absence of nanoparticles and that therefore these entities are not essential for crystal growth.

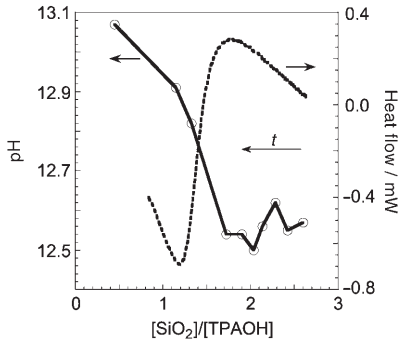

Figure 4. pH and heat flow from the crystallization of TPA/silicalite-1 solutions as a function of the composition of the liquid phase at 95 °C. The data, from Yang and Navrotsky,[30] have been plotted in terms of [SiO_2]/[TPAOH] in solution to facilitate comparison to plots presented in other figures. The composition of the liquid phase has been determined from the mass of crystals formed at given times, and the known initial composition (TPAOH/SiO_2/H_2O/C_2H_5OH 9:25:480:100). See Table 1 and Figure 5 in ref. [30]. The position of the transition is 1.4 SiO_2/TPAOH, not 1.0 as predicted by the models, but this may reflect that the collection of the zeolite crystals from the solution is not quantitative.[30]

Silica Condensation Models

The experimental observations described above can be explained semiquantitatively by a simple silica condensation model.[32] The model is similar to the ones used to describe surfactant self-assembly into micelles (within the pseudo-phase separation approximation)[33] with the addition of the acid-base chemistry of silica as described by the following equations:

$$Si(OH)_4(aq) \overset{K_a^1}{\rightleftharpoons} Si(OH)_3O^-(aq) + H^+(aq) \quad (1)$$

$$Si(OH)_4(aq) \overset{K_c}{\rightleftharpoons} \frac{1}{n}Si_nO_{4n-m}H_{4n-2m} + \frac{m}{n}H_2O \quad (2)$$

$$\equiv SiOH \overset{K_{a,np}}{\rightleftharpoons} \equiv SiO^- + H^+ \quad (3)$$

$$H_2O \overset{K_W}{\rightleftharpoons} OH^- + H^+ \quad (4)$$

where $[\equiv SiOH] = n[Si_nO_{4n-m}H_{4n-2m}]$; K_a^1 = first dissociation constant of silicic acid (H_4SiO_4) [mol L^{-1}], K_c = condensation constant for the formation of nanoparticles from silicic acid [mol L^{-1}], $K_{a,np}$ = effective dissociation constant of silanol groups in the nanoparticles [mol L^{-1}], K_W = dissociation constant of water, n = number of silicon atoms in the nanoparticle. Equation (2) describes the formation of nanoparticles of size n and assumes the silica is in Q^3 coordination ($Q^3 = Si(OSi)_3OH$). The model has only one fitting parameter, the effective dissociation constant of silanol groups in the nanoparticles [$K_{a,np}$, Eq. (3)]. This parameter has been fitted to one of the curves of Figure 5 ($pK_{a,np}$ = 11.2) and was then used to predict the behavior of the system pH for all compositions. The agreement to experiment is nearly quantitative for all compositional space sampled. The differences between experimental and predicted pH below the locus of cac are due to the simplicity of the model that considers one silica species (H_4SiO_4), while in fact there are many silica oligomers in solution,[34–37] and considers only the first deprotonation of silicic acid while, in effect, at high pH the silicic acid can have two silanol groups dissociated simultaneously.[38] Note that although the speciation of silica is very complex and depends on the cations in solution, this seems to have only minor effects on pH. For example, the data in Figure 5 for TPAOH solutions are identical to curves obtained in TMAOH/SiO_2 solutions.

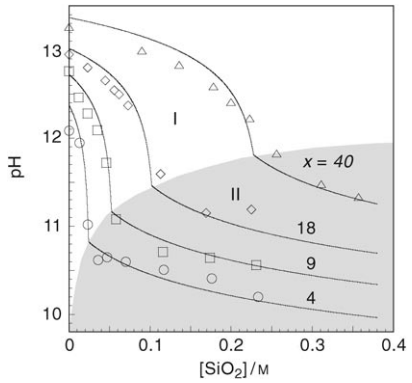

Figure 5. pH of TPAOH solutions at different silica concentrations (symbols) and comparison to the predictions of the silica condensation model (lines).[32] The shaded region is the area where nanoparticles are observed and the line separating the graph in two regions is a locus of cac. The model predicts that in region I the concentration of nanoparticles is very small. In region II the concentration of nanoparticles increases monotonically with additional silica (see Figure 7). The value of $pK_{a,np}$ was obtained from fitting the model to the curve with composition TPAOH/H_2O 9:9500. The values of the parameters are: $pK_a^1 = 9.5$, $pK_c = -2.98$, and $n = 356$ (see ref. [32]).

The high value estimated for the effective $pK_{a,np}$ constant for nanoparticle silanol groups is contrary to the expectation that condensation of silicic acid should lead to species that are *more* acidic than the monomer. However, a particle containing multiple charges will generate an electrostatic potential (ψ) with a maximum value at the particle surface (Figure 6). This potential will change the local concentration of hydrogen and hydroxide anions in the vicinity of the particle surface (and inside the particle if the particles are porous) leading to an apparently high value of $pK_{a,np}$ (within the framework of this model). This effect can be corrected by determining the electrostatic potential explicitly (through the Poison–Boltzmann equation[32]) and using Equations (5) and (6):

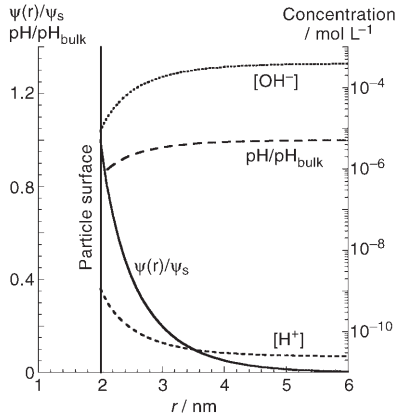

Figure 6. Spatial variation of electrostatic potential, $\psi(r)$, the concentration of hydrogen [H^+] and hydroxide [OH^-] ions and pH from the surface of a negatively-charged spherical particle (4 nm in diameter). The calculations have been conducted for solutions of composition TPAOH/SiO_2/H_2O/C_2H_5OH 9:9:9500:36 for a surface potential of $\psi_S = -98$ mV. The potential distribution is calculated numerically using the Poisson–Boltzmann equation and the local concentration of ions determined by using Equation (5) (see ref. [32] and [34]). Note the substantial change in hydrogen and hydroxide ion concentration near the particle surface. The pH in the bulk is $pH_{bulk} = 10.6$ and at the surface is $pH_S = 9.1$.

$$[H^+]_S = [H^+]_\infty e^{-(e\psi_S/k_BT)} \quad (5)$$

$$K_{a,np} = K_{a,np}^{corr} \cdot e^{-(e\psi_S/k_BT)} = \frac{[\equiv SiO^-][H^+]_\infty}{[\equiv SiOH]} \quad (6)$$

where e = electric charge of an electron, $[H^+]_S$ = hydrogen ion concentration at the nanoparticle surface [mol L^{-1}], $[H^+]_\infty$ = bulk hydrogen ion concentration [mol L^{-1}], ψ_S = electrostatic potential at the particle surface [V], $K_{a,np}^{corr}$ = effective dissociation constant of silanol groups in the nanoparticles corrected for the effect of the electrostatic potential at the particle surface [mol L^{-1}], $[\equiv SiO^-]$ = concentration of dissociated nanoparticle silanol groups per unit of volume of solution [mol L^{-1}], $[\equiv SiOH]$ = concentration of nanoparticle silanol groups per unit of volume of solution [mol L^{-1}], k_B is the Boltzmann constant.

Values near $\psi_S = -100$ mV or even lower at high pH have been determined for the surface potentials at the particle surface. The intrinsic $pK_{a,np}^{corr}$ has been recalculated to account for the local concentration of hydrogen ions near the particle surface leading to more reasonable values ($pK_{a,np}^{corr} = 8.4$). Thus, once the local effects of the electrostatic potential are considered, the condensation model fits experimental observations with physically realistic parameters.

The success of this simple condensation model is important at several levels. First, it makes a connection between the formation of these inorganic oxide particles and the formation of surfactant micelles. This analogy indicates that in the inorganic system there are forces that tend to increase the size of the particles and forces that tend to decrease the size of the particles, and it is the balance between these forces that gives rise to uniform and stable nanoparticles in solution.[25] The forces that lead to aggregation are clearly dominated by the formation of Si-O-Si bonds,[20] but the forces that lead to a decrease in size are less clear. The free energy associated with the formation of a diffuse double layer outside (and inside) the particles has been suggested as an important component of this latter element.[32] Second, the model helps to predict the concentration of silica species in the system under conditions that are inaccessible experimentally. For instance, it predicts the concentration of (neutral) H_4SiO_4, which is important because it specifies the chemical potential of individual species in solution.[33] The chemical potential provides, in turn, the driving force for processes of practical importance such as crystallization of zeolites or dense silica phases.[38] Formally, growth rates should be related to the concentration of this species provided crystal growth is slow compared with the rate of chemical exchange between silica in solution and silica in the nanoparticles. Figure 7 shows how the concentration of H_4SiO_4 changes as a function of composition and shows that most of the monomeric silica is deprotonated both prior to and after the cac. On the contrary, most of the silanol groups in the nanoparticles are not dissociated. This is the result of the large variation in electrostatic potential in the solutions that stems from the coupling of the acid–base chemistry of silanol groups and the diffuse double layer.

The model also helps to understand changes in solution properties during zeolite synthesis in molecular terms. For example, the change in enthalpy of dissolution of TEOS at the cac (Figure 3) can now be understood simply as a change in the main reaction, that is, before the cac silica forms monomers and oligomers in solution [that are for the most part charged, as in Eq. (1)], but after the cac silica forms nanoparticles that are, for the most part, neutral [Eq. (3)]. At the same time, the model helps understand the transition from an exothermic to an endothermic crystal growth process as the pool of reagents changes from nanoparticles (exothermic) to dissolved silica (endothermic).

It should be pointed out that many of the elements needed to develop these models have been known for decades. For example, Iler states in his book that a … "Solution of sodium or potassium silicate with SiO_2/M_2O molar ratios of 1:1 and 1:2 consists mainly of SiO_3^{2-} and $HSiO^-$ ions. However, in solutions of higher ratios it is proposed that an increasing proportion of the silica forms extremely small three-dimensional, internally condensed silicate polymer-ions or charged particles … [and that] these particles are in solubility equilibrium with soluble silica monomer, $Si(OH)_4$, which in turn is in equilibrium with monomeric silicate ions."[20] … Early work by Vail,[39,40] Stumm,[41] and Iler focused on the solubility of silicate solutions—citing changes in both pH and conductivity as a function of silica concentration—analogous to the data presented in Figure 3b and 5. However, not until recently have these findings been fully understood within the context of self-assembly.

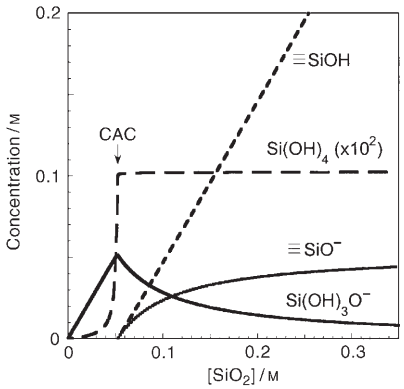

Figure 7. Concentration of H_4SiO_4, $H_3SiO_4^-$, and nanoparticle silica species (≡SiOH and ≡SiO^-) as a function of the total concentration of silica (initial composition: TPAOH/H_2O 9:9500). There are essentially no nanoparticles before the cac and beyond this point the concentration of particles increases monotonically. The model also shows that the concentration of soluble silica species decreases monotonically after the cac. Note that most of the silica in solution is charged while most of the silanol group in the nanoparticles are not dissociated. Also note that the concentration of H_4SiO_4 is nearly constant after the cac. Zeolite growth rates in this region are constant as a function of the *total* concentration of silica[24] providing experimental support to the idea that the concentration of H_4SiO_4 is controlling the growth rates.

Evolution of Nanoparticles upon Heating

In the above discussion we omitted any description of the changes in the nanoparticles upon increasing the temperature and it remains to be determined if the general picture of stable nanoparticles is still accurate at zeolite synthesis temperatures. It has been established that upon heating the particles grow slightly by an Ostwald ripening mechanism and the number density decreases accordingly.[42] The pH and conductivity increase slightly suggesting high-temperature particles are more condensed than the low temperature particles, but there is currently no direct evidence for this change in connectivity, for example, from ^{29}Si NMR spectroscopy. Importantly, the location of the cac appears not to change much for temperatures below 95 °C and thus the phase diagram depicted in Figure 5 is still a valid approximation to the microstructure of silica in the liquid phase during crystal nucleation and growth.

From Nanoparticles to Extended Structures

The long-term stability of silica/TPA nanoparticles is a reflection of repulsive interparticle forces that keep particles separated from each another at room temperature. Since the particles are negatively charged, there is evidently electrostatic repulsion between the particles. There is, however, another component of the repulsive forces that may be dominant at high pH where the ionic strength of the solutions is high.

Figure 8 compares the pair distance distribution function (PDDF) of silica/TPA particles measured by SAXS and SANS. The effective particle size is clearly different for the two scattering radiations and reveals a core–shell structure with silica mainly in the core, and TPA in the shell. This TPA shell is effectively a Stern layer of adsorbed cations on the particle surface.[34]

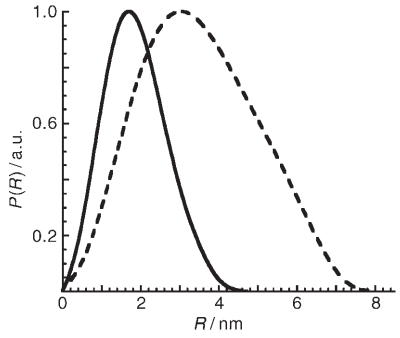

Figure 8. X-ray and neutron pair distance distribution functions (PDDF) from a solution of composition $TPAOD/SiO_2/D_2O/C_2H_5OD$ 9:40:9500:160 containing silica nanoparticles. The differences between the two curves reveal a core–shell structure where the core is composed mostly of silica and the shell is formed mostly of TPA. In this system X-rays are scattered primarily by silica whereas neutrons are scattered by both silica and TPA cations. The size of the particles can be easily determined as the point where the PDDF goes to zero. SAXS (——), SANS (-----).

Since the TPA layer has an effective electron density similar to water, its contribution to attractive van der Waals interparticle forces is small.[34] Upon collision between these core–shell particles the forces between the particles will remain repulsive as the large size of the shell keeps the silica cores far enough apart as to make the attractive core–core forces ineffective.[43] But the forces between layers of organic cations can be manipulated by changing the size and structure of the organic moiety. If the cations are amphiphilic, the hydrophobic end of the molecule can order in the Stern layer leading to attractive (hydrophobic) forces between nanoparticles.[25] If particles aggregate, one could observe a solid phase formed upon reaching the cac, a phase that may or may not have periodic order.[44] This is plainly what is observed in the synthesis of M41S[45,46]-type materials with organic cations such as cetyltrimethylammonium. There is then a fundamental connection between silica nanoparticles detected in zeolite synthesis and the synthesis of mesoporous materials. The attractive and repulsive force balance between nanoparticles is thus of enormous practical consequence and it is an area that deserves much more attention since by choosing the structure of the cation, it is possible to engineer the behavior of saturated silica solutions like the ones described here.

Structure Direction in Zeolite Synthesis

A key element of structure direction is the ability to transfer geometric and size information from the structure director to the silica phase.[47] It is rather surprising that in the scheme presented above, there is no instance where clear, direct contact between the structure director (TPA^+) and the silica phase is detected. The organic cation is observed always as a shell in the nanoparticles, but not changing the structure of the silica. Not much is known about the details of the interface between the silica nanoparticles and the organic cations, but if the crystal structures of cubic silsesquioxanes hydrates are used as a guide,[48–50] one would expect a strongly bound layer of water molecules between the silanol/siloxi groups and the TPA cations.[51] It is also hard to imagine that concerted changes in the structure of the silica nanoparticles to form zeolite-like structures are feasible as this would entail simultaneous and coordinated breaking and forming of multiple Si-O-Si bonds in these highly cross-linked particles.

We have found that it is not until the system of TPA–silica nanoparticles is heated that there may be some occlusion of TPA molecules into the silica core. Higher temperatures seem to be essential to drive the cation and the silica into direct physical contact. Nevertheless, there is no evidence that the incorporation of TPA in the silica nanoparticles is leading to any zeolite-like subunits at low temperatures or short times that can be identified by optical spectroscopy.

The lack of van der Waals contacts between the structure-director and silica in these basic solutions can be contrasted to the fluoride-containing highly concentrated gels recently used by Camblor[52,53] and Corma[54] to prepare various new siliceous zeolites. Assuming that the fluoride ions are all associated with the silica, the composition of these gels can be described by $0.5\,[H_4SiO_4F]^-:0.5\,R^+:0.5\,[H_4SiO_4]:1–10\,H_2O$ (where R^+ is the structure director). This composition is reminiscent of an ionic liquid and forces very close contact between the organic cation and the silica (at the initial stages of the synthesis). This may be the reason why these groups have been so successful preparing new zeolite structures using this composition.

Is there any generality to the zeolite synthesis scheme that has been presented here? Many different organic cations have been studied and the formation of stable silica nanoparticles has been detected in all cases that zeolite-forming structure-directors have been used.[18,55,56] The initial step of silica self-assembly into nanoparticles appears to be very general. However, the easy formation of zeolite nuclei

at low temperatures (below 100 °C) from silica nanoparticles appears to be characteristic of silicalite-1 materials only. Chen and Shantz have investigated the formation of ZSM-12 and other siliceous zeolites with various organic cations and have not been able to prepare any crystalline materials at low temperatures.[56] It is not until higher temperatures (above 150 °C) are reached, that these other systems start to evolve into highly organized microporous frameworks. This is consistent with the occlusion of the structure director into silica as being an activated process and necessary for the onset of nucleation. Why silicalite-1 is different from other all-silica zeolite syntheses remains to be determined.

Final Remarks

Silica aggregation is a common process in basic aqueous solutions that can lead to particles or extended structures precisely like surfactant micelles. It is quite possible that other inorganic oxides (i.e., and mixtures thereof germania and titania) can show similar behaviour—an area deserving further study.

The silica condensation model discussed here is only a first approximation to describing the system as these structures have no definite size or shape, but a distribution about some mean value. The roles of the organic cation, solvent, and hydrogen bonding, and other solution non-idealities are still not included (thermodynamic theories of self-assembly and molecular modeling,[48,57] similar to the ones used for surfactant self-assembly, are needed to further understand the unique characteristics of the silica nanoparticles described here).[58] In particular, the connectivity of the nanoparticles is a measurable quantity that has not been determined, as a function of composition and temperature, that could greatly help understand the formation of the particles and their structural evolution from amorphous to crystalline nuclei.

Understanding how the organic cations get embedded within the particles seems to be the crucial step to identifying the process of structure direction in these silica phases. Careful, molecular-level measurements of this evolution should be part of experimental studies in the future to clarify how zeolite nuclei are actually formed.

While our analysis of the experiments of Yang and Navrotsky indicates that growth of zeolites may proceed by addition of monomers, the direct addition of nanoparticles has not been excluded at other conditions.[59] A predictive model that accounts for all processes of silicalite-1 crystallization is still lacking.

Acknowledgements

This work was funded in part by the National Science Foundation through the Nanoscale Interdisciplinary Research Team (NIRT) under Grant CTS-0103010 and also under Grant DMR-0404153. We are grateful to S. Yang and A. Navrotsky for providing the raw data for Figure 4.

[1] C. S. Cundy, P. A. Cox, *Chem. Rev.* **2003**, *103*, 663–701.
[2] M. E. Davis, *Nature* **2002**, *417*, 813–821.
[3] R. F. Lobo, *Introduction to the Structural Chemistry of Zeolites*, in Handbook of Zeolite Science and Technology (Eds.: S. M. Auerbach, K. A. P. Carrado, M. Dutta), Marcel Dekker, New York, **2003**, 1084.
[4] A. J. Corma, *J. Catalysis* **2003**, *216*, 298–312.
[5] K. Tanabe, W. F. Holderich, *Appl. Catal. A* **1999**, *181*, 399–434.
[6] S. I. Zones, S. J. Hwang, S. Elomari, I. Ogino, M. E. Davis, A. W. Burton, *Comptes Rendus Chimie* **2005**, *8*, 267–282.
[7] International Zeolite Association, Database of Zeolite Structures, http://www.iza-structure.org/databases/
[8] J. N. Watson, L. E. Iton, J. W. White, *Chem. Commun.* **1996**, 2767–2768.
[9] P. de Moor, T. P. M. Beelen, R. A. van Santen, *J. Phys. Chem. B* **1999**, *103*, 1639–1650.
[10] R. Ravishankar, C. E. A. Kirschhock, P. P. Knops-Gerrits, E. J. P. Feijen, P. J. Grobet, P. Vanoppen, F. C. De Schryver, G. Miehe, H. Fuess, B. J. Schoeman, P. A. Jacobs, J. A. Martens, *J. Phys. Chem. B* **1999**, *103*, 4960–4964.
[11] B. J. Schoeman, O. Regev, *Zeolites* **1996**, *17*, 447–456.
[12] P. M. Piccione, C. Laberty, S. Y. Yang, M. A. Camblor, A. Navrotsky, M. E. Davis, *J. Phys. Chem. B* **2000**, *104*, 10001–10011.
[13] F. Schüth, W. Schmidt, *Adv. Mater.* **2002**, *14*, 629–638.
[14] A. Navrotsky, *Proc. Natl. Acad. Sci. USA* **2004**, *101*, 12096.
[15] J. Hedlund, S. Mintova, J. Sterte, *Microporous Mesoporous Mater.* **1999**, *28*, 185–194.
[16] S. Y. Yang, A. Navrotsky, *Chem. Mater.* **2004**, *16*, 3682–3687.
[17] J. M. Fedeyko, J. D. Rimer, R. F. Lobo, D. G. Vlachos, *J. Phys. Chem. B* **2004**, *108*, 12271–12275.
[18] J. M. Fedeyko, D. G. Vlachos, R. F. Lobo *Langmuir* **2005**, *21*, 5197–5206.
[19] B. J. Schoeman, *Microporous Mater.* **1997**, *9*, 267–271.
[20] R. K. Iler, *The Chemistry of Silica*, Wiley, New York, **1979**.
[21] S. Mintova, N. H. Olson, J. Senker, T. Bein, *Angew. Chem.* **2002**, *114*, 2670–2673; *Angew. Chem. Int. Ed.* **2002**, *41*, 2558–2561.
[22] C. E. A. Kirschhock, D. D. Liang, A. Aerts, C. A. Aerts, S. P. B. Kremer, P. A. Jacobs, G. Van Tendeloo, J. A. Martens, *Angew. Chem.* **2004**, *116*, 4662–4664; *Angew. Chem. Int. Ed.* **2004**, *43*, 4562–4564.
[23] H. Ramanan, E. Kokkoli, M. Tsapatsis, *Angew. Chem.* **2004**, *116*, 4658–4661; *Angew. Chem. Int. Ed.* **2004**, *43*, 4558–4561.
[24] V. Nikolakis, E. Kokkoli, M. Tirrell, M. Tsapatsis, D. G. Vlachos, *Chem. Mater.* **2000**, *12*, 845–853.
[25] J. Israelachvili, *Intermolecular and Surface Forces*, Academic Press, New York, **1992**.
[26] P. de Moor, T. P. M. Beelen, R. A. van Santen, K. Tsuji, M. E. Davis, *Chem. Mater.* **1999**, *11*, 36–43.
[27] P. de Moor, T. P. M. Beelen, B. U. Komanschek, O. Diat, R. A. van Santen, *J. Phys. Chem. B* **1997**, *101*, 11077–11086.
[28] S. Y. Yang, A. Navrotsky, D. J. Wesolowski, J. A. Pople, *Chem. Mater.* **2004**, *16*, 210–219.
[29] B. J. Schoeman, *Zeolites* **1997**, *18*, 97–105.
[30] S. Y. Yang, A. Navrotsky, *Chem. Mater.* **2002**, *14*, 2803–2811.
[31] C. H. Cheng, D. F. Shantz, *J. Phys. Chem. B* **2005**, *109*, 13912–13920.
[32] J. D. Rimer, D. G. Vlachos, R. F. Lobo, *Langmuir* **2005**, *21*, 8960–8971
[33] D. F. Evans, H. Wennerström, *The Colloidal Domain: Where Physics, Chemistry, Biology and Technology Meet*, 2nd ed., Wiley, New York, **1999**.
[34] P. C. Hiemenz, R. Rajagopalan, *Principles of Colloid and Surface Chemistry*, Marcel Dekker, New York, **1997**.
[35] A. V. McCormick, A. T. Bell, C. J. Radke, *Zeolites* **1987**, *7*, 183–190.
[36] H. C. Marsmann, R. Lower, *Chem. Ztg.* **1973**, *97*, 660.
[37] G. Engelhardt, D. Michel, *High-resolution solid-state NMR of silicates and zeolites*, Wiley, New York, **1987**.

[38] *Silica: Physical Behavior, Geochemistry, and Materials Applications* (Eds.: P. J. Heaney, C. T. Prewitt, G. V. Gibbs), Mineralogical Society of America, Washington, DC, **1994**.
[39] J. G. Vail, *Soluble Silicates in Industry*, Chemical Catalog Company, New York, **1928**.
[40] J. G. Vail, *Soluble Silicates their Properties and Uses*, Reinhold, New York, **1952**.
[41] W. Stumm, J. J. Morgan, *Aquatic chemistry—An introduction emphasizing chemical equilibria in natural waters*, Wiley-Interscience, New York, **1970**.
[42] J. D. Rimer, D. G. Vlachos, R. F. Lobo, *J. Phys. Chem. B* **2005**, *109*, 12762–12771.
[43] P. Claesson, R. G. Horn, R. M. Pashley, *J. Colloid Interface Sci.* **1984**, *100*, 250–263.
[44] J. M. Fedeyko, D. G. Vlachos, R. F. Lobo, *Micropor. Mesopor. Mater.* **2005**, in press.
[45] J. S. Beck, J. C. Vartuli, W. J. Roth, M. E. Leonowicz, C. T. Kresge, K. D. Schmitt, C. T. W. Chu, D. H. Olson, E. W. Sheppard, S. B. McCullen, J. B. Higgins, J. L. Schlenker, *J. Am. Chem. Soc.* **1992**, *114*, 10834–10843.
[46] J. C. Vartuli, C. T. Kresge, M. E. Leonowicz, A. S. Chu, S. B. McCullen, I. D. Johnsen, E. W. Sheppard, *Chem. Mater.* **1994**, *6*, 2070–2077.
[47] M. E. Davis, R. F. Lobo, *Chem. Mater.* **1992**, *4*, 756–768.
[48] S. Caratzoulas, D. G. Vlachos, M. J. Tsapatsis, *J. Phys. Chem. B* **2005**, *109*, 10429–10434.
[49] M. Wiebcke, J. Felsche, *Microporous Mesoporous Mater.* **2001**, *43*, 289–297.
[50] M. Wiebcke, D. J. Hoebbel, *J. Chem. Soc. Dalton Trans.* **1992**, 2451–2455.
[51] H. Koller, R. F. Lobo, S. L. Burkett, M. E. Davis, *J. Phys. Chem.* **1995**, *99*, 12588–12596.
[52] M. J. Diaz-Cabanas, M. A. Camblor, Z. Liu, T. Ohsuna, O. J. Terasaki, *Mater. Chem.* **2002**, *12*, 249–257.
[53] M. A. Camblor, P. A. Barrett, M. J. Diaz-Cabanas, L. A. Villaescusa, M. Puche, T. Boix, E. Perez, H. Koller, *Microporous Mesoporous Mater.* **2001**, *48*, 11–22.
[54] J. A. Vidal-Moya, T. Blasco, F. Rey, A. Corma, M. Puche, *Chem. Mater.* **2003**, *15*, 3961–3963.
[55] P. de Moor, T. P. M. Beelen, R. A. van Santen, L. W. Beck, M. E. Davis, *J. Phys. Chem. B* **2000**, *104*, 7600–7611.
[56] C. H. Cheng, D. F. Shantz, *J. Phys. Chem. B* **2005**, *109*, 7266–7274.
[57] M. Jorge, S. M. Auerbach, P. Monson, *J. Am. Chem. Soc.* **2005**, *127*, in press.
[58] D. Blankschtein, A. Shiloach, N. Zoeller, *Curr. Opin. Colloid Interface Sci.* **1997**, *2*, 294–300.
[59] I. Diaz, E. Kokkoli, O. Terasaki, M. Tsapatsis, *Chem. Mater.* **2004**, *16*, 5226–5232.

Published online: November 28, 2005

